Adaptive H-Infinity Filter Design for State of Charge Estimation on Lithium-Ion Battery Based on the Third-Order Equivalent Circuit Model

1st Haritsyam Anshari
Department of Electrical Engineering
Faculty of Engineering, Universitas Indonesia
Depok 16424, West Java, Indonesia
haritsyam.anshari@ui.ac.id

2nd Dr. Ir. Aries Subiantoro, S.T., M.Sc.
Department of Electrical Engineering
Faculty of Engineering, Universitas Indonesia
Depok 16424, West Java, Indonesia
biantoro@eng.ui.ac.id

***Abstract*—Lithium-ion batteries have been widely used in energy storage and electrical power sources. The advantages of lithium-ion batteries include higher power density, higher open-circuit voltage, faster charging process, lower maintenance, and a longer lifespan compared to other types of rechargeable batteries. When using lithium-ion batteries, Battery Management System (BMS) is required to control the charging and discharging process to prevent overcharing and undercharging. This way, the battery has higher efficiency, a longer lifespan, and its operational safety is guaranteed. In BMS, State of Charge (SoC) is an important parameter in battery monitoring and management. The parameter is used to estimate the remaining charge of the battery cells. SoC cannot be measured directly via external electrical signals, and both relate to internal chemical parameters within the battery. However, SoC can be measured through certain algorithms through measurable parameters, such as voltage and current. This paper presents the design of Adaptive H-Infinity Filter (AHIF) based on the 3rd Order Equivalent Circuit Model (ECM). Furthermore, AHIF is known for its robustness while the 3rd Order ECM is expected to be more accurate in representing the battery internal dynamics.**

Keywords—State of Charge (SoC), lithium-ion battery (Li-ion), Adaptive H-Infinity Filter (AHIF), Third-Order Equivalent Circuit Model (3rd ECM)

I. INTRODUCTION

Environmental degradation has become a major problem in the world. One of which is global warming which has become the center of attention in the industrial and academic fields. Through Paris Agreement guidelines, countries have attempted to reduce emissions and save energy [46], In this effort, it can be predicted that the transition in the transportation sector to the use of electricity-based energy will occur. This includes an increasing trend in the use of electric vehicles (EVs).

Lithium-ion batteries have been widely used in energy storage and power sources since the first commercial rechargeable lithium-ion battery was produced in 1991. Its use as energy storage is in line with the increasing trend of electric vehicle (EV) use. The advantages of lithium-ion batteries include higher power density, higher open voltage value, faster charging process, lower maintenance requirements, and longer life span compared to other types of rechargeable batteries, such as lead-acid (Pb), nickel-metal hydride (Ni-MH), and nickel-cadmium (Ni-Cd) batteries [51]. The advantages of lithium-ion batteries make them the best candidate for use in electric vehicles (EV).

The use of lithium-ion batteries is followed by the need for a Battery Management System (BMS) to control battery operations. In BMS, the State of Charge (SoC) parameter is known as an indicator of battery charging level. However, SoC cannot be measured directly, but is estimated through measurable battery parameters, such as voltage and current. This makes accurate SoC estimation important in the use of BMS to avoid overcharging or discharging in its operation. That way, the battery has higher efficiency, a longer life span, and guarantees battery operational safety.

SoC estimation methods in battery cells include direct measurement, book-keeping, model-based methods, and data-based methods [2]. Some direct measurement methods are the Open Circuit Voltage (OCV), internal resistance (IR), and impedance spectroscopy (IS) methods. In addition, book-keeping methods include Coulomb Counting and its variations [2].

Model-based methods and data-based methods are types of SoC estimation methods that are common in research focus. Data-based methods utilize artificial neural network construction with various developments and variations in their architecture. Data-based methods include variations of Neural Network (NN), such as Convolutional Neural Network (CNN), Deep Neural Network (DNN), Extreme Learning Machine (ELM), DDRN-NARX, to Long Short-Term Memory (LSTM). Not limited to NN variations, data-based methods also include Support Vector Regression (SVR) and Lightning Search Algorithm (LSA).

In model-based methods, a model is needed that represents the battery, such as an electrochemical model (EM) and an equivalent circuit model (ECM). In the electrochemical model, chemical and electrical reactions in the battery cell are considered. However, the electrochemical model is complex, so it tends to have a high computation time. ECM is a type of battery model that is commonly used, such as in the Kalman Filter-based estimation method. In the literature, the type of ECM that is popularly used for SoC estimation is the first or second order type. This is because the Third Order is considered too complex and has a long mathematical derivation. For this reason, this study tries to fill this literature gap.

Model-based methods include variations of the Kalman Filter (KF), such as the Extended Kalman Filter (EKF), Unscented Kalman Filter (UKF), to variations of the Kalman Filter with adaptive features. In addition, various variations of the PI Observer development, Sliding Mode Observer, to Moving Horizon Estimation are also categorized as model-based methods.

Another alternative SoC estimation method is the H-Infinity Filter (HIF), as in [53]. The use of HIF is based on the minimax error criterion which is expected to be more robust from model and measurement uncertainty. This study focuses

on adaptive variations of HIF. Thus, it is expected that the SoC estimation determined through this method is more accurate.

II. Problem Statement

Thus, this study regarding model-based SoC estimation faces four main challenges, namely:

A. Battery Model Parameter Identification

With the use of ECM as a battery model, the physical values of the battery (resistances and capacitances) are time-variant due to the battery's internal dynamics. So, an online parameter identification method is needed to ensure the model remains accurate throughout the cell life cycle. In addition, higher order ECM, such as the 3rd order, is preferable for solving model uncertainty problems.

B. Measurement Noise and Initial Value Offset

Current and voltage measurements are affected by noise. Furthermore, initial value SoC with high offset can lead to accumulated estimation deviations. Therefore, estimation methode that are robust to noise and robust to initial condition uncertainty is needed.

C. SoC-Voc Function Construction

Open circuit voltage is a function of SoC. SoC-Voc function is needed on the output function in model-based SoC estimation methods. The function must be modeled appropriately to ensure estimation accuracy.

III. Battery Modelling and Identification

A 3rd Order ECM can be illustrated as follows:

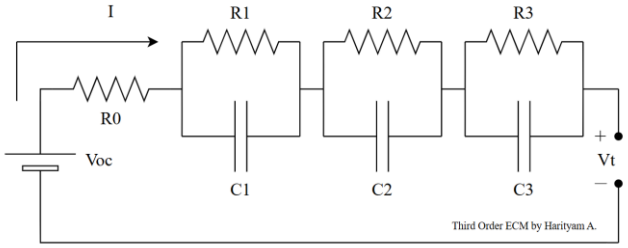

Figure 1 3rd Order ECM Circuit Diagram

In that diagram, V_{oc} represents the open circuit voltage, V_t represents the terminal voltage, I represents the discharging current, R_i represents the resistance with $i = 0, 1, 2, 3$, and C_i represents the capacitance with $i = 1, 2, 3$.

A 3rd Order ECM can be expressed in domain frequency as follows:

$$V_t(s) = V_{oc}(s) - R_0 \cdot I(s) - \frac{R_1}{sR_1C_1+1} \cdot I(s) - \frac{R_2}{sR_2C_2+1} \cdot I(s) - \frac{R_3}{sR_3C_3+1} \cdot I(s) \quad (3.1)$$

To form the transfer function, the system output is represented by the difference between the terminal voltage and the open circuit voltage as follows:

$$G(s) = \frac{V_t(s)-V_{oc}(s)}{I(s)} = -\left(R_0 + \frac{R_1}{sR_1C_1+1} + \frac{R_2}{sR_2C_2+1} + \frac{R_3}{sR_3C_3+1}\right) \quad (3.2)$$

The transfer function can be simplified as follows:

$$G(s) = -\frac{n_3s^3+n_2s^2+n_1s+n_0}{m_3s^3+m_2s^2+m_1s+1}$$

$$n_3 = R_0 \cdot \tau_1\tau_2\tau_3$$

$$n_2 = R_0(\tau_1\tau_2 + \tau_1\tau_3 + \tau_2\tau_3) + R_1(\tau_2\tau_3) + R_2(\tau_1\tau_3) + R_3(\tau_1\tau_2)$$

$$n_1 = R_0(\tau_1 + \tau_2 + \tau_3) + R_1(\tau_2 + \tau_3) + R_2(\tau_1 + \tau_3) + R_3(\tau_1 + \tau_2)$$

$$n_0 = R_0 + R_1 + R_2 + R_3$$

$$m_3 = \tau_1\tau_2\tau_3$$

$$m_2 = \tau_1\tau_2 + \tau_1\tau_3 + \tau_2\tau_3$$

$$m_1 = \tau_1 + \tau_2 + \tau_3 \quad (3.3)$$

Where $\tau_i = R_iC_i$ for $i = 1, 2, 3$.

Next, a discrete transformation is performed using the Tustin method as follows:

$$G(z^{-1}) = \frac{a_1+a_2z^{-1}+a_3z^{-2}+a_4z^{-3}}{b_1+b_2z^{-1}+b_3z^{-2}+b_4z^{-3}} \quad (3.4)$$

The a and b coefficient will not be described for simplicity. The discrete transfer function can be transformed into a difference equation as follows:

$$y(k) = \frac{a_1}{b_1}u(k) + \frac{a_2}{b_1}u(k-1) + \frac{a_3}{b_1}u(k-2) + \frac{a_4}{b_1}u(k-3) - \frac{b_2}{b_1}y(k-1) - \frac{b_3}{b_1}y(k-2) - \frac{b_4}{b_1}y(k-3) \quad (3.5)$$

The final difference equation is determined by reinserting the values of V_t, V_{oc}, and I. It is assumed that $V_{oc}(k) = V_{oc}(k-1)$ considering the flat characteristics of the SoC-Voc curve.

$$V_t(k) = \frac{b_1+b_2+b_3+b_4}{b_1}V_{oc} - \frac{b_2}{b_1}V_t(k-1) - \frac{b_3}{b_1}V_t(k-2) - \frac{b_4}{b_1}V_t(k-3) + \frac{a_1}{b_1}I(k) + \frac{a_2}{b_1}I(k-1) + \frac{a_3}{b_1}I(k-2) + \frac{a_4}{b_1}I(k-3) \quad (3.6)$$

Then, the regression model for RLS can be determined from the difference equation above as follows:

$$\varphi = [1, \ V_t(k-1), \ V_t(k-2), \ V_t(k-3), \ I(k), \ I(k-1), \ I(k-2), \ (k-3)]$$

$$\theta = [\frac{b_1+b_2+b_3+b_4}{b_1}V_{oc}; \ -\frac{b_2}{b_1}; \ -\frac{b_3}{b_1}; \ -\frac{b_4}{b_1}; \ \frac{a_1}{b_1}; \ \frac{a_2}{b_1}; \ \frac{a_3}{b_1}; \ \frac{a_4}{b_1}]$$

$$V_t(k) = \varphi(k) \cdot \theta^{\mathrm{T}}(k) \quad (3.7)$$

Recursive Least Squared is performed on the regression model above with the algorithm shown on Table 1.

The discrete transfer function can be substituted with the regression parameters as follows; this is done to simplify mathematical derivation.

$$G(z^{-1}) = \frac{\theta_5+\theta_6z^{-1}+\theta_7z^{-2}+\theta_8z^{-3}}{1-\theta_2z^{-1}-\theta_3z^{-2}-\theta_4z^{-3}} \quad (3.8)$$

With the V_{oc} can be calculated as follows:

$$V_{oc} = \frac{\theta_1}{1-\theta_2-\theta_3-\theta_4} \quad (3.9)$$

Table 1 Recursive Least Squared Algorithm

RECURSIVE LEAST SQUARE (RLS) ALGORITHM	
1	Initialize for $k = 0$ $\varphi_0, \theta_0, P_0, \lambda_0$
2	For every iteration $k = 1, 2, \ldots$ Calculate error $\epsilon(k)$: $\epsilon(\mathrm{k}) = \mathrm{y(k)} - \varphi(\mathrm{k})\,\theta(\mathrm{k}-1)$ Calculate covariance matrix $P(k)$: $P(k) = \frac{1}{\lambda}P(k-1)\left[I - \frac{\varphi(k)\varphi(k)^{\top}P(k-1)}{\lambda + \varphi(k)^{\top}P(k-1)\varphi(k)}\right]$ Update regression vector: $\hat{\theta}(k) = \hat{\theta}(k-1) + P(k)\,\varphi(k)\,\varepsilon(k)$

The discrete transfer function described by the regression parameters is transformed back to the frequency domain form as follows:

$$G(s) = -\frac{p_3 s^3 + p_2 s^2 + p_1 s + p_0}{q_3 s^3 + q_2 s^2 + q_1 s + 1}$$

$$q_3 = \frac{T^3}{8}\cdot\frac{1+\theta_2-\theta_3+\theta_4}{1-\theta_2-\theta_3-\theta_4}$$

$$q_2 = \frac{T^2}{4}\cdot\frac{3+\theta_2+\theta_3-3\theta_4}{1-\theta_2-\theta_3-\theta_4}$$

$$q_1 = \frac{T}{2}\cdot\frac{3-\theta_2+\theta_3+3\theta_4}{1-\theta_2-\theta_3-\theta_4}$$

$$p_3 = \frac{T^3}{8}\cdot\frac{\theta_5-\theta_6+\theta_7-\theta_8}{1-\theta_2-\theta_3-\theta_4}$$

$$p_2 = \frac{T^2}{4}\cdot\frac{3\theta_5-\theta_6-\theta_7+3\theta_8}{1-\theta_2-\theta_3-\theta_4}$$

$$p_1 = \frac{T}{2}\cdot\frac{3\theta_5+\theta_6-\theta_7-3\theta_8}{1-\theta_2-\theta_3-\theta_4}$$

$$p_0 = \frac{\theta_5+\theta_6+\theta_7+\theta_8}{1-\theta_2-\theta_3-\theta_4} \tag{3.10}$$

Then, the coefficient m and n relate to the coefficient p and q to determine the relationship between the physical parameters through regression parameters.

Thus, the seven equations needed to determine the seven physical parameters (R_0, R_1, R_2, R_3, C_1, C_2, C_3) is as follows:

$$\tau_1\tau_2\tau_3 = \frac{T^3}{8}\cdot\frac{1+\theta_2-\theta_3+\theta_4}{1-\theta_2-\theta_3-\theta_4} \tag{3.11}$$

$$\tau_1\tau_2 + \tau_1\tau_3 + \tau_2\tau_3 = \frac{T^2}{4}\cdot\frac{3+\theta_2+\theta_3-3\theta_4}{1-\theta_2-\theta_3-\theta_4} \tag{3.12}$$

$$\tau_1 + \tau_2 + \tau_3 = \frac{T}{2}\cdot\frac{3-\theta_2+\theta_3+3\theta_4}{1-\theta_2-\theta_3-\theta_4} \tag{3.13}$$

$$R_0 = \frac{-\theta_5+\theta_6-\theta_7+\theta_8}{1+\theta_2-\theta_3+\theta_4} \tag{3.14}$$

$$R_1(\tau_2\tau_3) + R_2(\tau_1\tau_3) + R_3(\tau_1\tau_2) = -\frac{T^2}{4}\left(\frac{3\theta_5 - \theta_6 - \theta_7 + 3\theta_8 + R_0(3+\theta_2+\theta_3-3\theta_4)}{1-\theta_2-\theta_3-\theta_4}\right) \tag{3.15}$$

$$R_1(\tau_2+\tau_3) + R_2(\tau_1+\tau_3) + R_3(\tau_1+\tau_2) = -\frac{T}{2}\left(\frac{3\theta_5 + \theta_6 - \theta_7 - 3\theta_8 + R_0(3-\theta_2+\theta_3+3\theta_4)}{1-\theta_2-\theta_3-\theta_4}\right) \tag{3.16}$$

$$R_1 + R_2 + R_3 = \frac{-\theta_5-\theta_6-\theta_7-\theta_8}{1-\theta_2-\theta_3-\theta_4} - R_0 \tag{3.17}$$

A cubic equation with roots (τ_1, τ_2, τ_3) has the following form:

$$x^3 - (\tau_1+\tau_2+\tau_3)x^2 + (\tau_1\tau_2+\tau_1\tau_3+\tau_2\tau_3)x - \tau_1\tau_2\tau_3 = 0 \tag{3.18}$$

In this equation, all coefficients can be determined by the equations (3.11), (3.12), and (3.13). All the time constants (τ_1, τ_2, τ_3) can be solved using the Cardano Formula or the roots function in MATLAB simulation.

R_0 can be solved analytically in equation (3.14). R_1, R_2, and R_3 can be found using equation (3.15), (3.16), (3.17), and the time constants value found previously.

Equation (3.15), (3.16), and (3.17) are converted into matrix equation form such as:

$$A \cdot R = B$$

$$A = \begin{bmatrix} \tau_2\tau_3 & \tau_1\tau_3 & \tau_1\tau_2 \\ \tau_2+\tau_3 & \tau_1+\tau_3 & \tau_1+\tau_2 \\ 1 & 1 & 1 \end{bmatrix}$$

$$R_m = \begin{bmatrix} R_1 \\ R_2 \\ R_3 \end{bmatrix}$$

$$B = \begin{bmatrix} -\frac{T^2}{4}\left(\frac{3\theta_5 - \theta_6 - \theta_7 + 3\theta_8 + R_0(3+\theta_2+\theta_3-3\theta_4)}{1-\theta_2-\theta_3-\theta_4}\right) \\ = -\frac{T}{2}\left(\frac{3\theta_5 + \theta_6 - \theta_7 - 3\theta_8 + R_0(3-\theta_2+\theta_3+3\theta_4)}{1-\theta_2-\theta_3-\theta_4}\right) \\ \frac{-\theta_5-\theta_6-\theta_7-\theta_8}{1-\theta_2-\theta_3-\theta_4} - R_0 \end{bmatrix} \tag{3.18}$$

Matrix A is determined from the time constant value while Matrix B is determined from the regression parameters and R_0. Thus, all the remaining resistance (R_1, R_2, R_3) are determined by solving for Matrix R_m.

With all the known time constant and resistance values, capacitances are determined as follows:

$$C_i = \frac{\tau_i}{R_i} \text{ for } i = 1, 2, 3 \tag{3.19}$$

IV. ADAPTIVE H-INFINITY FILTER FOR SOC ESTIMATION

The AHIF algorithm utilizes the following battery system model:

$$x_{k+1} = Ax_k + Bu_k + w_k$$
$$y_k = Cx_k + Du_k + v_k \tag{3.20}$$

$$x_k = \begin{bmatrix} SoC(k) \\ V_1(k) \\ V_2(k) \\ V_3(k) \end{bmatrix} \tag{3.21}$$

$$u_k = I_k \tag{3.22}$$

$$A = \begin{bmatrix} 1 & 0 & 0 & 0 \\ 0 & e^{-\frac{T}{R_1C_1}} & 0 & 0 \\ 0 & 0 & e^{-\frac{T}{R_2C_2}} & 0 \\ 0 & 0 & 0 & e^{-\frac{T}{R_3C_3}} \end{bmatrix} \tag{3.23}$$

$$B = \begin{bmatrix} -\eta \cdot \frac{T}{Q_b} \\ R_1\left(1 - e^{-\frac{T}{R_1 C_1}}\right) \\ R_2\left(1 - e^{-\frac{T}{R_2 C_2}}\right) \\ R_3\left(1 - e^{-\frac{T}{R_3 C_3}}\right) \end{bmatrix} \quad (3.24)$$

$$C = \begin{bmatrix} \frac{d\,Voc}{d\,SoC} & -1 & -1 & -1 \end{bmatrix} \quad (3.25)$$

$$D = [-R_0] \quad (3.26)$$

$$\hat{y}_k = \hat{V}_t = h(x_k, u_k) = \mathrm{Voc(SoC)} - I_k R_0 - V_{1,k} - V_{2,k} - V_{3,k} \quad (3.27)$$

The Adaptive H-Infinity Filter (AHIF) algorithm is a development of the conventional H∞ Filter (HIF) method by adding an adaptation mechanism to the dynamics of noise and system parameters boldly (online). AHIF is designed to maintain the stability of the estimate despite the brightness of the model, unknown measurement noise, or variations in system parameters.

Unlike the Extended Kalman Filter (EKF) which relies on the assumption of Gaussian noise and linear covariance propagation, and the H∞ Filter (HIF) which focuses on dampening the effects of disturbances using the H∞ norm without statistical assumptions, AHIF adds adaptation to the process noise covariance (Q) and measurement (R) in real-time based on the moving average of the error innovations (residuals).

The Adaptive H-Infinity Filter Algorithm as follows:

Table 2 Adaptive H-Infinity Filter (AHIF) Algorithm

ADAPTIVE H-INFINITY FILTER (AHIF) ALGORITHM [55]	
1	Initialization: For $k = 0$, initialize $\hat{x}_0$, P_0, S_0, L, Q_0, and R_0.
2	Time update for $k = 1, 2, 3, \ldots$
3	Update parameters $R_0, R_1, R_2, R_3, C_1, C_2, C_3$ from RLS.
4	Apriori state estimation: $\hat{x}_k^- = A_{k-1}\hat{x}_{k-1} + B_{k-1}u_{k-1}$
5	Apriori covariance estimation: $P_k^- = A_{k-1}P_{k-1}^+ A_{k-1}^T + Q_{k-1}$
6	Update positive definite symmetric matrix $\bar{S}_k$: $\bar{S}_k = L_k^T S_k L_k$
7	Calculate estimation of $\hat{y}_k$: $\hat{y}_k = \mathrm{Voc}(SoC_k) - I_k R_0 - \hat{V}_{1,k} - \hat{V}_{2,k} - \hat{V}_{3,k}$
8	Calculate *error* e_k: $e_k = y_k - \hat{y}_k$
9	Update measurement noise covariance matrix R_k: $\hat{M}_k = \frac{1}{N}\sum_{j=k-N+1}^{k} e_j e_j^T$ $\hat{R}_k = \hat{M}_k - C_k P_k^T C_k^T$
10	Update gain matrix: $K_k = A_k P_k^- (I - \theta \bar{S}_k P_k^- + C_k^T R_k^{-1} C_k P_k^-)^{-1} C_k^T R_k^{-1}$
11	Update process noise covariance matrix Q_k: $\hat{Q}_k = K_k \hat{M}_k K_k^T$
12	Update state vector posterior: $\hat{x}_k^+ = \hat{x}_k^- + K_k e_k$
13	Update covariance matrix posterior: $P_k^+ = P_k^- (I - \theta \bar{S}_k P_k^- + C_k^T R_k^{-1} C_k P_k^-)^{-1}$
14	Output
15	Wait for the next time sample at restart at step **3**.

V. SoC-Voc Function Construction

Open circuit voltage (V_{oc}) is a function of SoC. The SoC-Voc function can be determined by processing the low incremental OCV dataset available through *CALCE Battery Data* [52].

The battery used in this study is a $LiFePO_4$ battery type A123 with a rated capacity of 1100 mAh acquired from *CALCE Battery Data.* The low incremental OCV provides the values of two variables, battery voltage (V_t) and battery current (I) with respect to time. The dataset are divided into charge and discharge sections.

The SoC values are acquired from the current data. The current value is processed into SoC data through coulomb counting method (CC).

The open-circuit voltage (V_{oc}) values are acquired from the battery voltage (V_t). The open circuit voltage can be assumed to be the same as the battery voltage due to low current values or 0.055 A. However, this assumption may result in some offsets in the SoC-Voc that must be normalized.

Then, the charge and discharge SoC-Voc curves are averaged to determine the final SoC-Voc curve. The SoC-Voc function can be determined through polynomial fitting or look-up table. In this study, the eight order polynomial fitting is implemented.

VI. Results and Discussion

Simulation for SoC-Voc function construction is done in MATLAB script. Meanwhile, simulation for battery model parameter identification with RLS and SoC estimation with AHIF is done in MATLAB Simulink using level 1 s-function block. The result and discussion section will be divided into three parts, namelu the results of SoC-Voc function construction, the results of battery model parameter identification through RLS, and the results of SoC estimation through AHIF compared to EKF and HIF with CC as its reference SoC value.

A. SoC-Voc Function Construction

Using a polynomial fit of order 8 on the SoC-Voc curve obtained from the low-incremental OCV dataset, the SoC-Voc function is determined as follows:

$$V_{oc}(SoC) = -1097.9 \cdot SoC^8 + 4909.5 \cdot SoC^7 - 9072.5 \cdot SoC^6 + 8952.3 \cdot SoC^5 - 5086.1 \cdot SoC^4 + 1671.9 \cdot SoC^3 - 303.3 \cdot SoC^2 + 27.2 \cdot SoC + 2.3 \quad (4.1)$$

This function will be used in the nonlinear state space model of the battery, as in equation (3.27).

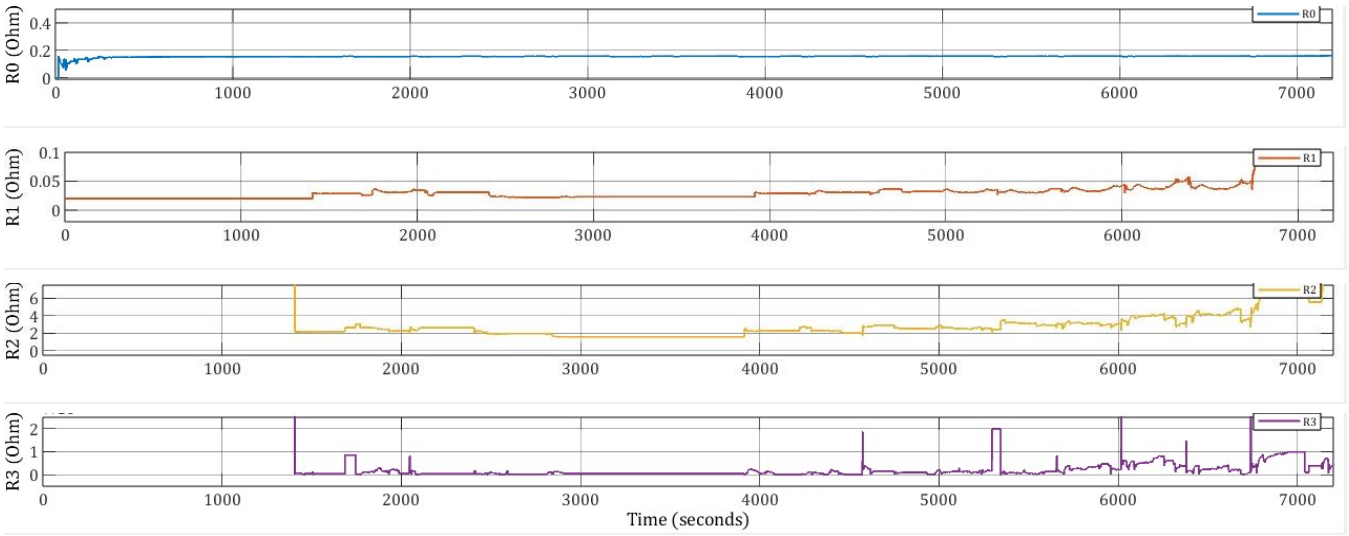

Figure 2 Resistance Acquired from RLS

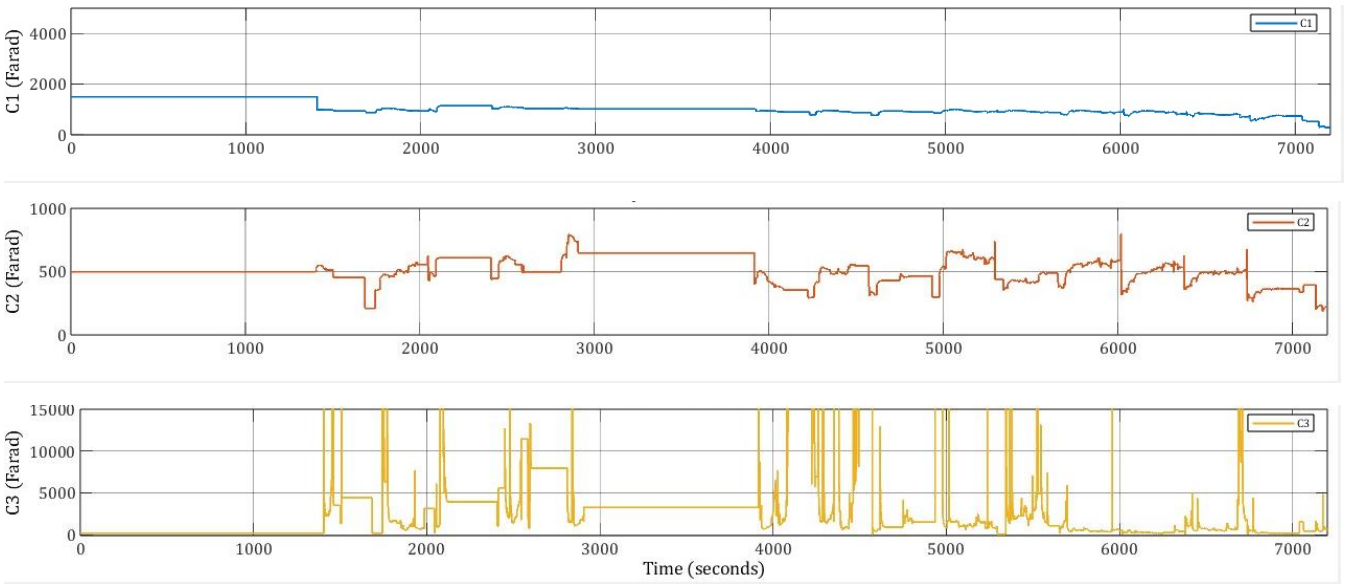

Figure 3 Capacitance Acquired from RLS

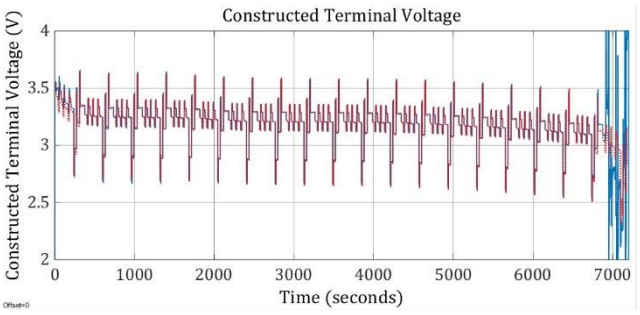

Figure 4 Battery Voltage Constructed from Physical Parameters

B. Battery Model Parameter Identification

In the battery model parameter identification, the driving cycle is provided by *CALCE Battery Dataset* for $LiFePO_4$ battery type A123 with a rated capacity of 1100 mAh. The driving cycle used in this study is DST 7200 seconds.

The results of resistance and capacitance values through RLS are shown in Figure 2 and Figure 3.

However, converting the regression parameters to physical parameters has notable weakness, namely the emergence of complex roots when the regression parameter values are unstable in the time constant cubic equation step. To handle this, a hold to last value mechanism is used where when a time constant is detected as a complex root, the calculation will utilize the previous time constant value. This phenomenon is seen at the early times of the simulation, in the range of 0-1500 seconds, where the physical parameter values are still constant.

From Figure 2, it is found R_0 is stable at a value of $0.1 - 0.2$ Ohm. R_1 value is stable in the range of $0.025 - 0.05$ Ohm and R_2 is stable in the range of $0.002 - 0.004$ Ohm before both values increase drastically at the end of the simulation time. R_3 is notably spikes in the range of $0 - 0.001$ Ohm.

From Figure 3, it is found C_1 stabilizes at the value 1000 Farad, C_2 stabilizes at the value $200 - 800$ Farad, C_3 seems unstable.

The construction of the terminal voltage output through physical parameters (*tegangan konstruksi parameter fisik*) and the RLS open voltage value are shown in Figure 3 with RMSE 0.04504 (for the first 6500 seconds) compared to real terminal voltage dataset.

As seen at the end of the graph, the construction of terminal voltage is broken. This is due to the utilization of the open circuit voltage value from RLS. The RLS open circuit voltage is not valid for steep curves due to the assumption of the regression model.

Next, a comparison is explained between the performance of RLS for third-order ECM with the proposed regression parameter conversion scheme to physical parameters and the performance of second-order ECM with the analytical approach. In the second and third order parameter identification tests, both were found to have the same RLS terminal voltage output RMSE, which is 0.04504. However, there is a difference in the terminal voltage RMSE resulting from parameter construction as follows:

Table 3 Second Order and Third Order Comparison

2ND ORDER AND 3RD ORDER COMPARISON ON VT ESTIMATION	
N-th Order	**RMSE**
RMSE Vt 2nd Order	0.04918
RMSE Vt 3rd Order	0.04567

C. SoC Estimation with AHIF

In SoC estimation, AHIF is used with EKF and HIF as a comparison. In addition, CC is used as the SoC reference value. CC is valid as a reference value if the input current in the simulation does not contain any noise.

In the following section are the tuning parameters for SoC estimation using AHIF:

Table 4 Tuning Parameters for SoC Estimation

TUNING PARAMETER FOR SOC ESTIMATION	
Method	**Parameter**
AHIF	$Q_0 = \begin{bmatrix} 10^{-8} & 10^{-5} \\ 10^{-5} & 10^{-5} \end{bmatrix}$ $R_0 = 10^{-4}$ $P_0 = \begin{bmatrix} 10^{-4} & 10^{-2} \\ 10^{-2} & 10^{-2} \end{bmatrix}$ $SoC_0 = 0.9$ $S_0 = I_{4x4}$ $\theta = 10^{-2}$ $N = 20$

The results regarding estimated SoC, terminal voltage (V_t), voltage V_1, voltage V_2, and voltage V_3 are shown in the graph below:

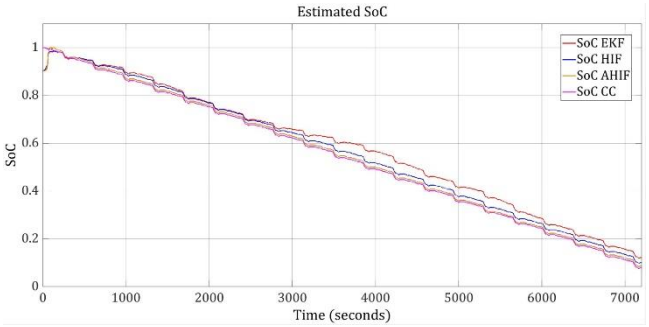

Figure 5 Estimated SoC on DST

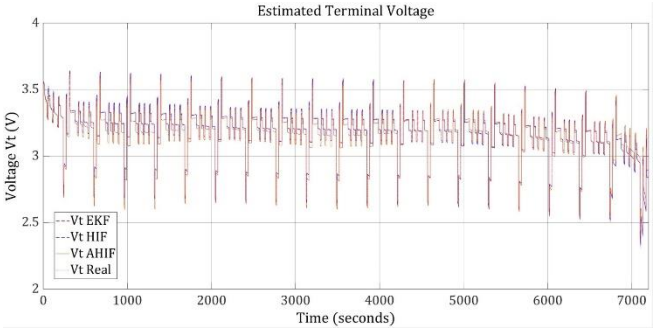

Figure 6 Estimated Terminal Voltage

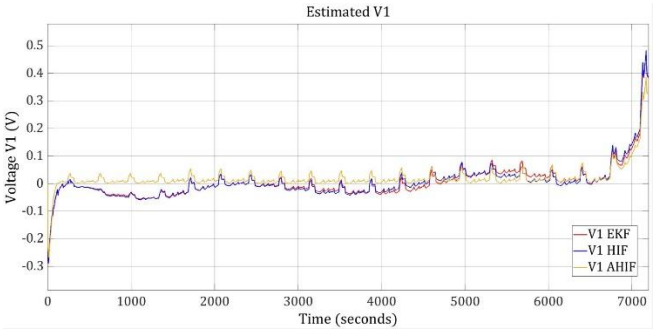

Figure 7 Estimated V1

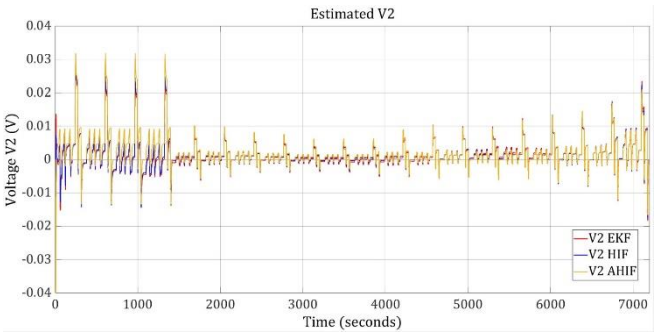

Figure 8 Estimated V2

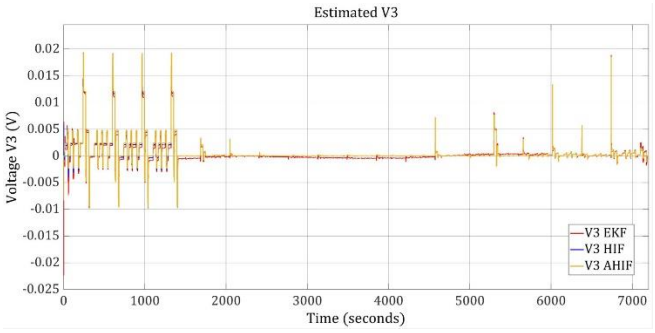

Figure 9 Estimated V3

Through the SoC results in Figure 5, the three SoC estimation techniques have well followed the actual SoC pattern.

All three SoC estimation techniques estimate battery terminal voltage measurements with high performance as seen in Figure 6. However, AHIF seems to have some offset. Meanwhile, EKF and HIF can follow the actual voltage well.

Meanwhile, all three estimators show similar performance and patterns in V_1, V_2, and V_3 estimations. However, AHIF has a unique characteristic where the voltage appears more stable or flat as seen in Figure 8, Figure 9, and especially in Figure 7.

The performance of the three estimators is analyzed using the RMSE error metric on the variables, SoC and terminal voltage, as follows:

Table 5 RMSE of SoC Estimation

RMSE OF SOC ESTIMATION		
Methode	**RMSE SoC**	**RMSE V_t**
EKF	0.04622	0.005511
HIF	0.02242	0.005919
AHIF	0.01069	0.0365

With the above results, Adaptive H-Infinity Filter (AHIF) and H-Infinity Filter (HIF) show the best performance compared to the EKF method. Then, EKF and HIF show better performance in estimating the terminal voltage V_t.

In addition, the use of AHIF also requires a greater computational load than other SoC estimation methods. Although the performance of the SoC estimation technique is quite good in simulation, the simulation process cannot simulate the battery degradation process that generally occurs in batteries over a long period of time. In addition, this SoC estimation study does not consider the effect of temperature that can change the shape of the SoC-Voc curve which is important in SoC estimation.

VII. CONCLUSSIONS

In this study, identification of battery model parameters is done by utilizing RLS and time constant cubic equation approach scheme in converting regression parameters to physical parameters. The error metric results with RMSE found are 0.04786 and the computational load is lighter compared to using nonlinear solver.

Regarding the polynomial fitting of the SoC-Voc curve, an 8th order polynomial fitting was used with an RMSE of 0.0482 when compared to the average SoC-Voc curve.

Adaptive H-Infinity Filter (AHIF) and H-Infinity Filter (HIF) show better performance compared to the EKF SoC estimation technique for DST load profiles. The RMSE of SoC through AHIF is 0.01069 and HIF is 0.02242 compared to EKF of 0.0462. This shows that AHIF and HIF have good performance, even when using the initial SoC value with offset.

Identification of battery model parameters generated by Third Order ECM using the time constant cubic equation approximation scheme is slightly more accurate compared to Second Order ECM. The performance of Third Order ECM is expected to be better if analytical equations are determined for the physical equations.

REFERENCES

[1] Kadem, O., & Kim, J. (2023). Real-Time State of Charge-Open Circuit Voltage Curve construction for battery state of charge estimation. *IEEE Transactions on Vehicular Technology*, *72*(7), 8613–8622. https://doi.org/10.1109/tvt.2023.3244623

[2] Lee, J., & Won, J. (2023). Enhanced coulomb counting method for SOC and SOH estimation based on coulombic efficiency. *IEEE Access*, *11*, 15449–15459. https://doi.org/10.1109/access.2023.3244801

[3] Misyris, G. S., Doukas, D. I., Papadopoulos, T. A., Labridis, D. P., & Agelidis, V. G. (2018). State-of-Charge estimation for Li-Ion batteries: A more accurate hybrid approach. *IEEE Transactions on Energy Conversion*, *34*(1), 109–119. https://doi.org/10.1109/tec.2018.2861994

[4] Partovibakhsh, M., & Liu, N. G. (2014). An adaptive unscented Kalman filtering approach for online estimation of model parameters and State-of-Charge of Lithium-Ion batteries for autonomous mobile robots. *IEEE Transactions on Control Systems Technology*, *23*(1), 357–363. https://doi.org/10.1109/tcst.2014.2317781

[5] Din, M. S. E., Hussein, A. A., & Abdel-Hafez, M. F. (2018). Improved battery SOC estimation accuracy using a modified UKF with an adaptive cell model under real EV operating conditions. *IEEE Transactions on Transportation Electrification*, *4*(2), 408–417. https://doi.org/10.1109/tte.2018.2802043

[6] Sun, Q., Lv, H., Wang, S., Gao, S., & Wei, K. (2021). Optimized state of charge estimation of Lithium-Ion battery in SMES/Battery hybrid energy storage system for electric vehicles. *IEEE Transactions on Applied Superconductivity*, *31*(8), 1–6. https://doi.org/10.1109/tasc.2021.3091119

[7] Obeid, H., Petrone, R., Chaoui, H., & Gualous, H. (2022). Higher order Sliding-Mode observers for State-of-Charge and State-of-Health estimation of Lithium-Ion batteries. *IEEE Transactions on Vehicular Technology*, *72*(4), 4482–4492. https://doi.org/10.1109/tvt.2022.3226686

[8] Haus, B., & Mercorelli, P. (2019). Polynomial augmented extended Kalman filter to estimate the state of charge of Lithium-Ion batteries. *IEEE Transactions on Vehicular Technology*, *69*(2), 1452–1463. https://doi.org/10.1109/tvt.2019.2959720

[9] Bianchi, V., Stighezza, M., Toscani, A., Chiorboli, G., & De Munari, I. (2023). An improved method based on support vector regression with application independent training for state of charge estimation. *IEEE Transactions on Instrumentation and Measurement*, *72*, 1–11. https://doi.org/10.1109/tim.2023.3306816

[10] Lin, T., Chen, Z., Zheng, C., Huang, D., & Zhou, S. (2020). Fault diagnosis of Lithium-Ion battery pack based on hybrid system and dual extended Kalman filter algorithm. *IEEE Transactions on Transportation Electrification*, *7*(1), 26–36. https://doi.org/10.1109/tte.2020.3006064

[11] Meng, J., Stroe, D., Ricco, M., Luo, G., & Teodorescu, R. (2018). A simplified Model-Based State-of-Charge estimation approach for Lithium-Ion battery with dynamic linear model. *IEEE Transactions on Industrial Electronics*, *66*(10), 7717–7727. https://doi.org/10.1109/tie.2018.2880668

[12] Li, R., Xu, S., Li, S., Zhou, Y., Zhou, K., Liu, X., & Yao, J. (2020). State of charge prediction algorithm of Lithium-Ion battery based on PSO-SVR cross validation. *IEEE Access*, *8*, 10234–10242. https://doi.org/10.1109/access.2020.2964852

[13] Cui, X., & Xu, B. (2021). State of charge estimation of Lithium-Ion battery using robust kernel fuzzy model and Multi-Innovation UKF algorithm under noise. *IEEE Transactions on Industrial Electronics*, *69*(11), 11121–11131. https://doi.org/10.1109/tie.2021.3121774

[14] Charkhgard, M., & Farrokhi, M. (2010). State-of-Charge estimation for Lithium-Ion batteries using neural networks and EKF. *IEEE Transactions on Industrial Electronics*, *57*(12), 4178–4187. https://doi.org/10.1109/tie.2010.2043035

[15] Wu, X., Li, X., & Du, J. (2018). State of charge estimation of Lithium-Ion batteries over wide temperature range using unscented Kalman filter. *IEEE Access*, *6*, 41993–42003. https://doi.org/10.1109/access.2018.2860050

[16] Huang, C., & Chow, M. (2021). Robust State-of-Charge estimation for Lithium-Ion batteries over full SOC range. *IEEE Journal of Emerging and Selected Topics in Industrial Electronics*, *2*(3), 305–313. https://doi.org/10.1109/jestie.2021.3078253

[17] Lipu, M. S. H., Hannan, M. A., Hussain, A., Saad, M. H., Ayob, A., & Uddin, M. N. (2019). Extreme Learning Machine Model for State-of-Charge Estimation of Lithium-Ion battery using gravitational

search Algorithm. *IEEE Transactions on Industry Applications*, *55*(4), 4225–4234. https://doi.org/10.1109/tia.2019.2902532

[18] Shen, J., Shen, J., He, Y., & Ma, Z. (2018). Accurate state of charge estimation with model mismatch for Li-Ion batteries: A Joint Moving Horizon Estimation approach. *IEEE Transactions on Power Electronics*, *34*(5), 4329–4342. https://doi.org/10.1109/tpel.2018.2861730

[19] Shen, J., He, Y., Ma, Z., Luo, H., & Zhang, Z. (2016). Online state of charge estimation of lithium-ion batteries: A moving horizon estimation approach. *Chemical Engineering Science*, *154*, 42–53. https://doi.org/10.1016/j.ces.2016.06.061

[20] Zhang, Z., Xue, B., & Fan, J. (2020). Noise Adaptive moving Horizon Estimation for State-of-Charge estimation of Li-Ion battery. *IEEE Access*, *9*, 5250–5259. https://doi.org/10.1109/access.2020.3047971

[21] Shen, P., Ouyang, M., Lu, L., Liu, J., & Feng, X. (2018). The co-estimation of state of charge, state of health, and state of function for lithium-ion batteries in electric vehicles. *Applied Energy, 206*, 978–988. https://doi.org/10.1016/j.apenergy.2017.09.104

[22] Chaoui, H., & Ibe-Ekeocha, C. C. (2017). State of charge and state of health estimation for lithium batteries using recurrent neural networks. *IEEE Transactions on Vehicular Technology, 66*(10), 8773–8783. https://doi.org/10.1109/TVT.2017.2715335

[23] He, Z., Yang, Z., Cui, X., & Li, E. (2020). A method of state-of-charge estimation for EV power lithium-ion battery using a novel adaptive extended Kalman filter. *Energy, 194*, 116841. https://doi.org/10.1016/j.energy.2019.116841

[24] He, L., Guo, D., Zhang, J., Li, W., & Zheng, Y. (2022). A threshold extended Kalman filter algorithm for state of charge estimation of lithium-ion batteries in electric vehicles. *Journal of Energy Storage, 45*, 103532. https://doi.org/10.1016/j.est.2021.103532

[25] Shi, Q., Jiang, Z., Wang, Z., Shao, X., & He, L. (2022). State of charge estimation by joint approach with model-based and data-driven algorithm for lithium-ion battery. *Energy Reports, 8*, 3505–3513. https://doi.org/10.1016/j.egyr.2022.02.224

[26] Hou, W., Shi, Q., Liu, Y., Guo, L., Zhang, X., & Wu, J. (2024). State of charge estimation for lithium-ion batteries at various temperatures by extreme gradient boosting and adaptive cubature Kalman filter. *Applied Energy, 358*, 121960. https://doi.org/10.1016/j.apenergy.2024.121960

[27] Kannan, M., Sundareswaran, K., Nyak, P. S. R., & Simon, S. P. (2023). A combined DNN-NBEATS architecture for state of charge estimation of lithium-ion batteries in electric vehicles. *IEEE Transactions on Transportation Electrification, 9*(2), 1784–1794. https://doi.org/10.1109/TTE.2022.3228171

[28] Jia, K., Gao, Z., & Gao, X. (2024). An adaptive LSTM network with fractional-order memory unit optimized by Hausdorff difference for SoC estimation of lithium-ion batteries. *Energy, 291*, 120365. https://doi.org/10.1016/j.energy.2024.120365

[29] Zhang, K., Ma, J., Zhao, X., Zhang, D., & He, Y. (2019). State of charge estimation for lithium battery based on adaptively weighting cubature particle filter. *Journal of Power Sources, 414*, 92–99. https://doi.org/10.1016/j.jpowsour.2019.01.065

[30] Kim, W., Lee, P.-Y., Kim, J., & Kim, K.-S. (2021). A robust state of charge estimation approach based on nonlinear battery cell model for lithium-ion batteries in electric vehicles. *IEEE Access, 9*, 32356–32365. https://doi.org/10.1109/ACCESS.2021.3060585

[31] Chen, X., Shen, W., Dai, M., Cao, Z., Jin, J., & Kapoor, A. (2016). Robust adaptive sliding-mode observer using RBF neural network for lithium-ion battery state of charge estimation in electric vehicles. *Applied Energy, 179*, 402–412. https://doi.org/10.1016/j.apenergy.2016.06.134

[32] Xu, J., Mi, C. C., Cao, B., Deng, J., Chen, Z., & Li, S. (2014). The state of charge estimation of lithium-ion batteries based on a proportional-integral observer. *IEEE Transactions on Vehicular Technology, 63*(4), 1614–1621. https://doi.org/10.1109/TVT.2013.2283667

[33] Xiong, R., Tian, J., Shen, W., & Sun, F. (2019). A novel fractional order model for state of charge estimation in lithium-ion batteries. *Energy, 166*, 397–407. https://doi.org/10.1016/j.energy.2018.10.078

[34] Wei, Y., & Ling, L. (2022). State-of-charge estimation for lithium-ion batteries based on temperature-based fractional-order model and dual fractional-order Kalman filter. *Journal of Power Sources, 521*, 230983. https://doi.org/10.1016/j.jpowsour.2021.230983

[35] Yu, Q., Huang, Y., Tang, A., Wang, C., & Shen, W. (2023). OCV-SOC-temperature relationship construction and state of charge estimation for a series parallel lithium-ion battery pack. *Energy, 264*, 126133. https://doi.org/10.1016/j.energy.2023.126133

[36] Yang, F., Song, X., Xu, F., & Tsui, K.-L. (2019). State-of-charge estimation of lithium-ion batteries via long short-term memory network. *IEEE Access, 7*, 19443–19453. https://doi.org/10.1109/ACCESS.2019.2897012

[37] Zhu, Q., Li, L., Hu, X., Xiong, N., & Hu, G.-D. (2017). H∞-based nonlinear observer design for state of charge estimation of lithium-ion battery with polynomial parameters. *Energies, 10*(4), 515. https://doi.org/10.3390/en10040515

[38] Shu, X., Chen, Z., Shen, J., Guo, F., Zhang, Y., & Liu, Y. (2023). State of charge estimation for lithium-ion battery based on hybrid compensation modeling and adaptive H-infinity filter. *Energy Reports, 9*, 1096–1105. https://doi.org/10.1016/j.egyr.2023.01.135

[39] Lipu, M. S. H., Hannan, M. A., Hussain, A., Saad, M. H. M., Ayob, A., & Blaabjerg, F. (2018). State of charge estimation for lithium-ion battery using recurrent NARX neural network model-based lighting search algorithm. *IEEE Access, 6*, 51253–51265. https://doi.org/10.1109/ACCESS.2018.2869220

[40] Liu, Z., Dang, X., & Jing, B. (2019). A novel open circuit voltage-based state of charge estimation for lithium-ion battery by multi-innovation Kalman filter. *Energies, 12*(4), 641. https://doi.org/10.3390/en12040641

[41] Dey, S., Mukherjee, S., Sharma, A., & Gupta, P. (2021). Advances in batteries, battery modeling, battery management system, battery thermal management, SOC, SOH, and charge–discharge characteristics: A review. *Journal of Energy Storage, 42*, 103054. https://doi.org/10.1016/j.est.2021.103054

[42] Omar, N., Monem, M. A., Firouz, Y., & Van Mierlo, J. (2013). State-of-the-art and energy management system of lithium-ion batteries in electric vehicle applications: Issues and recommendations. *Energies, 6*(12), 6464–6499. https://doi.org/10.3390/en6126464

[43] You, S., & Park, J. (2020). Lithium-ion battery pack robust state of charge estimation, cell inconsistency, and balancing: Review. *Journal of Energy Storage, 28*, 101283. https://doi.org/10.1016/j.est.2020.101283

[44] Eddahech, A., Briat, O., Bertrand, N., & Vinassa, J. M. (2012). An overview and comparison of online implementable SOC estimation methods for lithium-ion battery. *IEEE International Conference on Industrial Technology (ICIT)*, 1406–1411. https://doi.org/10.1109/ICIT.2012.6209984

[45] Hu, X., Li, S., & Peng, H. (2012). Overview of batteries state of charge estimation methods. *International Journal of Energy Research, 36*(4), 317–329. https://doi.org/10.1002/er.1861

[46] Zheng, Y., Zhu, J., & Jiang, B. (2020). Overview of model-based online state-of-charge estimation using Kalman filtering techniques. *Applied Sciences, 10*(22), 7969. https://doi.org/10.3390/app10227969

[47] Wang, Z., Lin, X., Zhao, Y., & Gong, Y. (2021). A review of lithium-ion battery state of charge estimation based on deep learning: Directions for improvement and future trends. *Journal of Energy Chemistry, 61*, 215–227. https://doi.org/10.1016/j.jechem.2021.01.015

[48] Xu, Y., Cao, H., & Liu, W. (2022). Real-time state of health estimation of lithium-ion batteries based on the equivalent internal resistance. *Energy Reports, 8*, 4019–4028. https://doi.org/10.1016/j.egyr.2022.03.133

[49] Song, Z., Li, J., Han, X., Ouyang, M., & Hofmann, H. (2017). A novel active equalization method for series-connected battery packs based on clustering analysis with genetic algorithm. *Energy, 124*, 186–195. https://doi.org/10.1016/j.energy.2017.02.064

[50] Wu, J., Liu, Y., Shi, Q., Guo, L., & Hou, W. (2023). Flexible battery state of health and state of charge estimation using partial charging data and deep learning. *Energy, 267*, 126504. https://doi.org/10.1016/j.energy.2023.126504

[51] Xu, Y., Zhou, X., Ma, T., & Cao, B. (2020). Robust estimation for state-of-charge and state-of-health of lithium-ion batteries using integral-type terminal sliding-mode observers. *IEEE Transactions on Industrial Electronics, 67*(4), 3012–3022. https://doi.org/10.1109/TIE.2019.2909872

[52] Center for Advanced Life Cycle Engineering (CALCE). (n.d.). *Battery data*. University of Maryland. Retrieved May 2, 2025, from https://calce.umd.edu/battery-data

[53] Chen, C., Xiong, R., & Shen, W. (2017). A Lithium-Ion Battery-in-the-Loop approach to test and validate multiscale dual H infinity filters for State-of-Charge and capacity estimation. *IEEE Transactions on Power Electronics*, *33*(1), 332–342. https://doi.org/10.1109/tpel.2017.2670081

[54] Engineering Educator Academy, Dr. Mehran Andalibi. (2024b, March 19). *Particle filter (Sequential Monte Carlo)* [Video]. YouTube. https://www.youtube.com/watch?v=tZ11uz-qphw

[55] Zhang, Y., Xiong, R., He, H., & Shen, W. (2016). Lithium-Ion battery pack state of charge and state of energy estimation algorithms using a Hardware-in-the-Loop validation. *IEEE Transactions on Power Electronics*, *32*(6), 4421–4431. https://doi.org/10.1109/tpel.2016.2603229

[56] D. Simon, "Optimal State Estimation: Kalman, H∞, and Nonlinear Approaches," Jan. 2006, doi: 10.1002/0470045345.ch11.

[57] B. Xia et al., "Strong tracking of a h-infinity filter in lithium-ion battery state of charge estimation," Energies (Basel), vol. 11, no. 6, p. 121693718, Jun. 2018, doi: 10.3390/en11061481.

[58] R. Yang, A. Zhang, L. Zhang, and Y. Hu, "A Novel Adaptive H-Infinity Cubature Kalman Filter Algorithm Based on Sage-Husa Estimator for Unmanned Underwater Vehicle," Math Probl Eng, vol. 2020, 2020, doi: 10.1155/2020/8057028.